# Omnidirectional Thermal Imaging Surveillance System Featuring Trespasser and Faint Detection

**Wai-Kit Wong**                                        wkwong@mmu.edu.my
*Faculty of Engineering and Technology,*
*Multimedia University,*
*75450 JLN Ayer Keroh Lama,*
*Melaka, Malaysia.*

**Zeh-Yang Chew**                                        chew5011@msn.com
*Faculty of Engineering and Technology,*
*Multimedia University,*
*75450 JLN Ayer Keroh Lama,*
*Melaka, Malaysia.*

**Hong-Liang Lim**                                        fly_dragon85@hotmail.com
*Faculty of Engineering and Technology,*
*Multimedia University,*
*75450 JLN Ayer Keroh Lama,*
*Melaka, Malaysia.*

**Chu-Kiong Loo**                                        ckloo@mmu.edu.my
*Faculty of Engineering and Technology,*
*Multimedia University,*
*75450 JLN Ayer Keroh Lama,*
*Melaka, Malaysia.*

**Way-Soong Lim**                                        wslim@mmu.edu.my
*Faculty of Engineering and Technology,*
*Multimedia University,*
*75450 JLN Ayer Keroh Lama,*
*Melaka, Malaysia.*

## Abstract

This paper proposed an efficient omnidirectional thermal imaging surveillance system featuring trespasser and faint detection. In this thermal imaging system, the omnidirectional scenes in a monitored site such as old folks home, nursing home, hospital etc. are first captured using a thermal camera attached to a custom made hyperbolic IR (infrared radiation) reflected mirror. The captured scenes to be monitored with trespasser or faint detection are then fed into a laptop computer for image processing and alarm purposes. Log-polar mapping is proposed to map the captured omnidirectional thermal image into panoramic image, hence providing the observer or image processing tools a complete wide angle of view. Two effective human behavioral detection algorithms namely: Human head detection algorithm and home alone faint detection algorithm are also designed for monitored the trespasser or fainted people detection. The observed significances of this new proposed omnidirectional thermal imaging system include: it can cover a wide angle of view (360º omnidirectional), using minimum hardware, low cost and the output thermal images are with higher data compression. Experimental results show that the proposed thermal imaging

surveillance system achieves high accuracy in detecting trespasser and monitoring faint detection for health care purpose.

**Keywords:** Monitoring and Surveillance, Thermal Imaging System, Trespasser Detection, Faint Detection, Omnidirectional System, Image Processing and Understanding.

## 1. INTRODUCTION
Conventional surveillance system that employs digital security cameras are great to keep residences safe from thief, vandalism, unwanted intruders and at the meantime can work as a health care facility for nursing purposes. However, such surveillance system normally employs human observers to analyze the surveillance video. Sometime this is more prone to error due to lapses in attention of the human observer [1]. There is a fact that a human's visual attention drops below acceptable levels when assigned to visual monitoring and this fact holds true even for a trained personnel [2],[3]. The weakness in conventional surveillance system has raised the need for a smart surveillance system where it employs computer and pattern recognition techniques to analyze information from situated sensors [4].

Another problem encountered in most conventional surveillance systems is the change in ambient light, especially in an outdoor environment where the lighting condition is varies naturally. This makes the conventional digital color images analysis task very difficult. One common approach to alleviate this problem is to train the system to compensate for any change in the illumination [5]. However, this is generally not enough for human detection in dark. In recent time, thermal camera has been used for imaging objects in the dark. The camera uses infrared (IR) sensors that capture IR radiation coming from different objects in the surrounding and forms IR image [6]. Since IR radiation from an object is due to the thermal radiation, and not the light reflected from the object, such camera can be conveniently used for trespasser or faint detection in night vision too.

Thermal imaging trespasser detection system is a type of smart surveillance system which is used to detect human objects (trespasser) even in poor lighting condition. The system can be employed to secure a place when and where human should not exist. A simple trespasser detection algorithm was proposed in [7]. The algorithm is regional based whereby an IR object that occupy more than certain number of partitions in a thermal image is considered as a human being and vice-versa. However, the algorithm is having two major concerns. First concern is distance, in which if a human being that is far away from the imaging system will not identified as a human. The second concern is if an animal (such as cat, dog etc.) is moving too close to the system (which occupy more than the threshold partitioned), it will be miss-considered as a human being too. Therefore, in this paper, a more effective trespasser detection algorithm with human head detection capability is proposed.

The second approach for the proposed omnidirectional thermal imaging surveillance system in this paper is with faint detection feature. Faint is one of the major problems that happen amongst the elderly people, patients or pregnant women which may cause them suffering physical injuries or even mental problems. Fainting normally occurs when the person falls and his or her head hits on the floor or on hard items. An emergency medical treatment for fainting mainly depends on the response and rescue time. Therefore, detection of faint incidents is very important in order to have the immediate treatment for this population. Various solutions have been developed to recognize faint motion. One of the common ways is using the wearable press button. This allows the person who had fall down to press the button to call for help. However, this system does not help if the person faint instantly. Furthermore, wearable faint motion sensor which makes use of the acceleration sensor and inclination sensor to recognize the motion automatically subsequently signals the alarm [8]. But, this system will not help if the person forgets to wear it. Thus, a possible solution is the use of automatic surveillance vision based systems.

Recently, thermal camera has been used for moving human detection [9], but it is not in omnidirectional view. If a single thermal camera is to monitor a single location, then for more

locations in different angle of view, there required more thermal cameras. Hence, it will cost more, beside complicated the surveillance network. In this paper, an effective surveillance system is proposed which includes three main features:

1) 360 degree viewing using a single thermal camera, surrounding location can be monitored. This achieving wide area coverage using minimum hardware.
2) Effective trespasser detection system able to detect trespassers, even in a poor lighting condition.
3) Effective automatic health care monitoring system that will raise alerts/alarm whenever any human fainted case arises.

Experimental results show that the proposed thermal imaging surveillance system achieves high accuracy in detecting trespasser and monitoring faint detection for health care purpose. The paper is organized as follows: Section 2 briefly comments on the omnidirectional thermal imaging surveillance system, section 3 summarizes log-polar image geometry and the mapping techniques for unwarping the captured omnidirectional thermal image into panoramic form. Then in section 4, it presents the proposed human head detection algorithm for trespasser detection and section 5 shows the home alone faint detection algorithm for health care surveillance purpose. Section 6 contains the experimental results. Finally in section 7 will draw conclusion and envison of future developments.

## 2. OMNIDIRECTIONAL THERMAL IMAGING SURVEILLANCE SYSTEM MODEL

The proposed omnidirectional thermal imaging surveillance system model in this paper is shown in Fig. 1. This system requires a custom made IR reflected hyperbolic mirror, a camera mirror holder, a fine resolution thermal camera and a laptop or personal computer installed with Matlab programming (version R2007b or later) and an alarm signaling system. The alarm signaling system can be as simple as a computer's speaker.
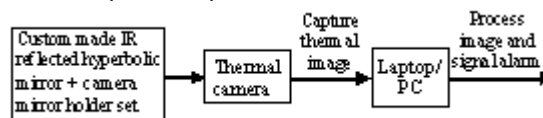


**FIGURE 1:** Omnidirectional Thermal Imaging Surveillance System Model

*A. Custom made IR reflected hyperbolic mirror*
The best shape of practical use omnidirectional mirror is hyperbolic. As derived by Chahl and Srinivasan in [10], all the polynomial mirror shapes (conical, spherical, parabolic, etc) do not provide a central perspective projection, except for the hyperbolic one. They also shown that the hyperbolic mirror guarantee a linear mapping between the angle of elevation $\theta$ and the radial distance from the center of the image plane $\rho$. Another advantage of hyperbolic mirror is when using it with a camera/imager of homogenous pixel density, the resolution in the omnidirectional image captured is also increasing with growing eccentricity and hence it will guarantee a uniform resolution for the panoramic image after unwarping.

The research group of OMNIVIEWS project from Czech Technical University further developed MATLAB software for designing omnidirectional mirror [11]. From the MATLAB software, omnidirectional hyperbolic mirror can be designed by inputting some parameters specify the mirror dimension. The first parameter is the focal length of the camera $f$, in which for the thermal camera in use is 12.5 mm and the distance $d$ ($\rho z$-plane) from the origin is set to 2 m. The image plane height $h$ is set to 20 cm. the radius of the mirror rim is chosen $t_1$=3.6cm as modified from Svoboda work in [12], with radius for fovea region 0.6 cm and retina region 3.0 cm. Fovea angle is set in between 0º to 45º, whereas retina angle is from 45º to 135º. The coordinates as well as the plot of the mirror shape is generated using MATLAB and shown in Fig. 2. The coordinates as well as mechanical drawing using Autocad are provided to precision engineering company to fabricate/custom made the hyperbolic mirror. The hyperbolic mirror is milling by using aluminum bar and then chrome plating with a chemical element named chromium. Chromium is regarded with great interest because of its lustrous (good in IR reflection), high corrosion resistance, high melting point and hardness. The fabricated mirror is shown in Fig. 3.
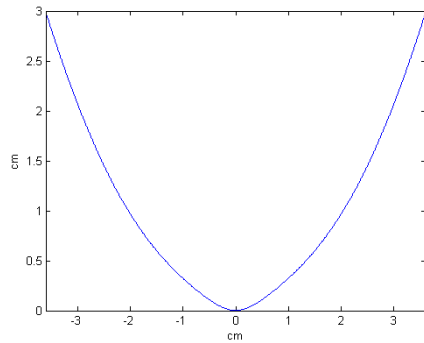
**FIGURE 2:** Mirror coordinates plot in MATLAB



**FIGURE 3:** Fabricated mirror

### B. Camera-mirror holder
The camera mirror holder is self designed and custom made with aluminum material as shown in Fig. 4.

### C. Thermal camera
The thermal camera used in this paper is an affordable and accurate temperature measurement mode: ThermoVision A-20M is manufactured by FLIR SYSTEM [13]. The thermal camera has a temperature sensitivity of 0.10 of range from -20ºC to 350ºC. However, for human detection, the temperature range is set to 30ºC to 40ºC. The thermal camera can capture thermal image with fine resolution up to 320 X 240 pixels offering more than 76,000 individual measurement points per image at a refresh rate of 50/60 Hz. The A-20M features a choice of connectivity options. For fast image and data transfer of real-time fully radiometric 16-bit images, an IEEE-1394 FireWire digital output can be chose. For network and/or multiple camera installations, Ethernet connectivity is also available. Each A-20M can be equipped with its own unique URL allowing it to be addressed independently via its Ethernet connection and it can be linked together with router to form a network. Therefore, it is best outfitted for human behavioral based surveillance system, such as trespasser and faint detection.

A problem encountered in thermal camera selection is the existence of the haloing effect in uncalibrated ferroelectric barium strontium titanate (BST) sensors. Haloing effect is the presence of halos around objects having a high thermal contrast with the background [14]. A-20M is chosen because it uses the uncooled microbolometer FPA detector technology which does not produce the haloing effect.

### D. Laptop/PC
A laptop or PC can be used for image processor, either place on site or in a monitoring room. Matlab ver R2007b programming is chosen to be used because it has user friendly software for performing log-polar mapping technique to unwrap the omnidirectional thermal image into panoramic form and it can partitioned the panoramic thermal images easily according to each single location to be monitored, process them smoothly with the trespasser or faint detection algorithm user programmed in, and alarm will be triggered once a human being is detected in a tested image for trespasser detection mode or faint motion is detected for faint detection mode. The overall fabricated system model is shown Fig. 4.

**FIGURE 4:** Overall fabricated omnidirectional thermal imaging surveillance system model

## 3. LOG-POLAR MAPPING

In this section, log-polar mapping is proposed for unwarping the captured omnidirectional thermal images into panoramic form providing the observer or image processing tools a complete wide angle of view. Log-polar geometry or log-polar transform in short, is an example of foveated or space-variant image representation used in the active vision systems motivated by human visual system [15]. It is a spatially-variant image representation in which pixel separation increases linearly with distance from a central point [16]. It provides a way of concentrating computational resources on regions of interest, whilst retaining low-resolution information from a wider field of view. One advantage of this kind of sampling is data reduction. Foveal image representations like this are most useful in the context of active vision system where the densely sampled central region can be directed to pick up the most salient information. Human eyes are very roughly organized in this way.

In robotics, there has been a trend to design and use true retina-like sensors [17], [18] or simulate the log-polar images by software conversion [19], [20]. In the software conversion of log-polar images, practitioners in pattern recognition usually named it as log-polar mapping. The advantages of log-polar mapping is that it can unwarp an omnidirectional image into panoramic image, hence providing the observer and image processing tools a complete wide angle of view for the surveillance area's surroundings and preserving fine output image quality in a higher data compression manner. The spatially-variant grid that represents log-polar mapping is formed by $i$ number of concentric circles with $N$ samples over each concentric circle [15]. An example of a spatially-variant sampling grid is shown in Fig. 5.

The log-polar mapping use in this paper can be summarized as following: Initially, omnidirectional thermal image is captured using a thermal camera and a custom made IR reflected hyperbolic mirror. The geometry of the captured omnidirectional thermal image is in Cartesian form $(x_1,y_1)$. Next, the Cartesian omnidirectional thermal image is sampled by the spatially-variant grid into a log-polar form $(\rho,\theta)$ omnidirectional thermal image. After that, the log-polar omnidirectional thermal image is unwarped into a panoramic thermal image $(x_2,y_2)$, another Cartesian form. Since the panoramic thermal image is in Cartesian form, subsequent image processing task will become much easier.

The center of pixel for log-polar sampling is described by [15]:

$$\rho(x_1, y_1) = \ln_b \left( \frac{R}{\rho_o} \right) \qquad (1)$$

$$\theta(x_1, y_1) = \left( \frac{N}{2\pi} \right) \tan^{-1} \left( \frac{y_1}{x_1} \right) \qquad (2)$$

The center of pixel for log-polar mapping is described as:

$$x_2(\rho, \theta) = \rho \, \cos \left( \frac{2\pi\theta(x_1, y_1)}{N} \right) \qquad (3)$$

$$y_2(\rho, \theta) = \rho \, \sin \left( \frac{2\pi\theta(x_1, y_1)}{N} \right) \qquad (4)$$

where R is the distance between given point and the center of mapping $= \sqrt{x_1^2 + y_1^2}$,

$\rho_o$ is the scaling factor which will define the size of the circle at $\rho(x_1, y_1) = 0$,
$b$ is the base of the algorithm [15],

$$b = \frac{N + \pi}{N - \pi} \qquad (5)$$

$N$ is the number of angular samples over each concentric circle.
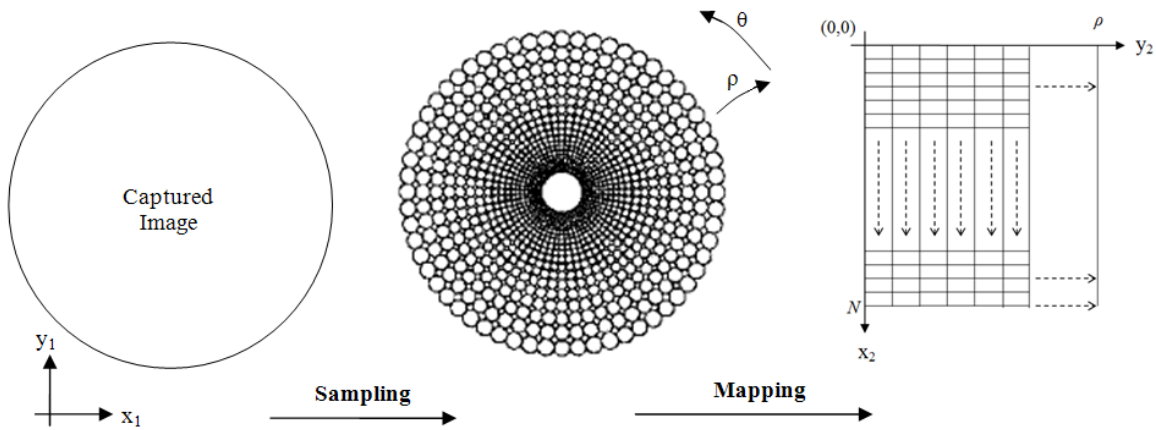


**FIGURE 7:** A graphical view of log-polar mapping.

A graphical view illustrating the log-polar mapping is shown in Fig. 5 [15]. To sample the Cartesian pixels $(x_1, y_1)$ into log-polar pixel $(\rho, \theta)$, at each center point calculated using (1) and (2), the corresponding log-polar pixel $(\rho_n, \theta_n)$ covers a region of Cartesian pixels with radius:

$$r_n = br_{n-1} \qquad (6)$$

where $n$ = 1,2,3,.....,$N$-1. Fig. 6 shows the circle sampling method of log-polar mapping [15], [21], where A, A', B and B' points are the centre of pixel for log-polar sampling.
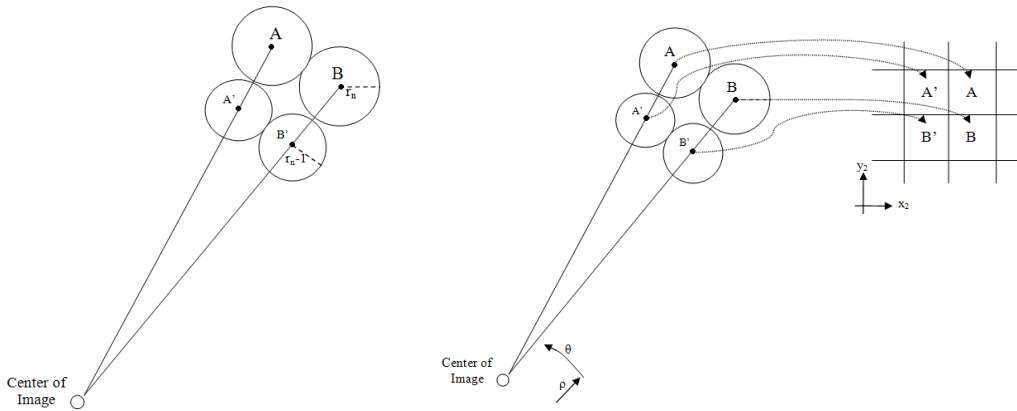
**FIGURE 8:** Circular Sampling Structure in Log-Polar Mapping.        Fig. 7. Unwarping Process.

The intensity value in each individual log-polar pixel equals the mean intensity value of all pixels inside the sampling circle on the original Cartesian image $(x_1,y_1)$:

$$mean = \frac{total \ (\ x_1, y_1\ ) \ pixel \ value}{total \ number \ of \ (\ x_1, y_1\ ) \ pixel} \qquad (7)$$

The region of Cartesian pixels on the panoramic image $(x_2,y_2)$ is covered by an individual log-polar pixel on the log-polar $(\rho,\theta)$ omnidirectional image. Therefore, the pixels in that specific region on the panoramic image $(x_2,y_2)$ will have the same intensity with respect to the corresponding individual log-polar pixel. Fig. 7 shows the mapping or unwarping of log-polar pixel onto its corresponding Cartesian pixel $(x_2,y_2)$, as described by (3) and (4).

## 4. HUMAN HEAD DETECTION ALGORITHM FOR TRESPASSER DETECTION
In this section, an effective trespasser detection algorithm modified from L.H.Lee's work in [22] is proposed. The proposed algorithm is discussed in detail as below.

   *A.   Algorithm for Trespasser Detection*
Step 1: Acquire thermal image through hyperbolic reflector. Please refer to Fig. 8 for the example of image captured.
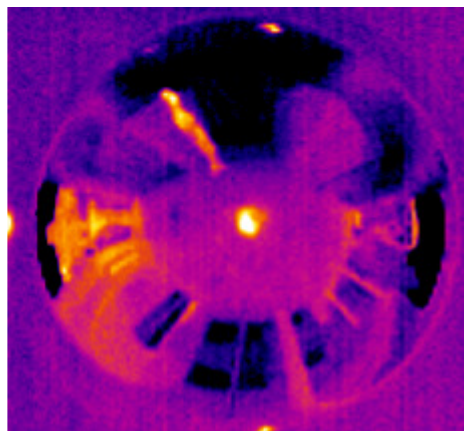


**FIGURE 8:** Thermal image captured through hyperbolic reflector

Step 2: Image unwarping: Unwarp the acquired thermal image into panoramic image. Please refer to Fig. 9 for the example on resulting panoramic image.
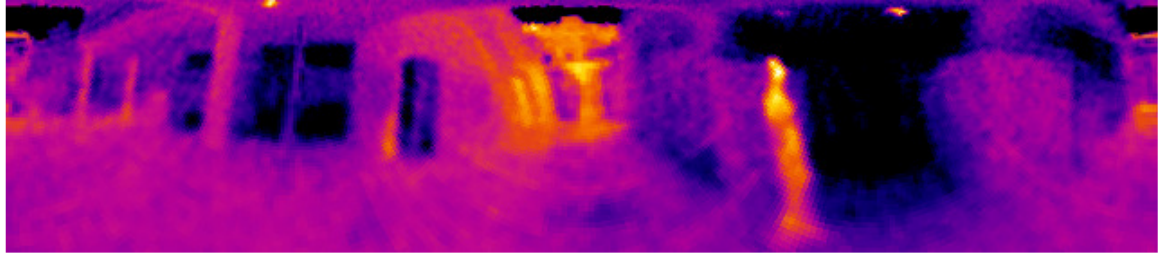
**FIGURE 9:** Panaromic view of the inspected scence after the thermal image is unwarpped

Step 3: Image cropping: Crop the image to obtain the thermal image of the interested area only. Please refer to Fig. 10 for the example on the resulting cropped image.
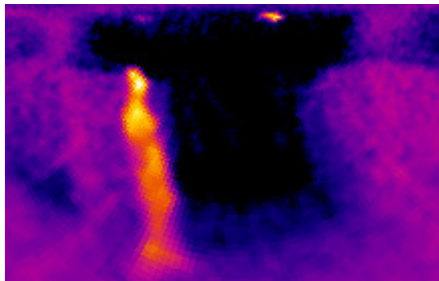


**FIGURE 10:** Thermal image after cropping process

Step 4: Binary image conversion: Convert Thermal image into purely black & white image (BW) using:

$$BW(i, j) = \begin{cases} 1, T_l \leq Temp(i, j) \leq T_h \\ 0, otherwise \end{cases} \quad (8)$$

Temp (i,j) = Temperature at point (i,j) of thermal image.
$T_l$ and $T_h$ are the minimum and maximum possible human body temperature.
i,j are the pixel's row and column coordinate respectively.

Step 5: Objects identification: Identify objects inside the BW where a group of discontinuous white pixels are considered as a single object.

Step 6: Boundary extraction: Find boundary line of each identified object inside BW and record it into an array of coordinates.

Step 7: Head detection: For each object's boundary, perform the Head detection algorithm as explained in section B.

Step 8: If human being is detected, trigger alarm.

*B. Algorithm for Head Detection*

Step 1: Starting point identification: Calculate the starting point for head top detection. The starting point shall be the highest point (smallest y-coordinate value) among the intersection points of the boundary with the horizontal middle line where horizontal middle line is given by x = $x_m$ and $x_m$ is the mean of all x-coordinates in the boundary of the object. Please refer Fig. 11(a) for better understanding.

Step 2: Peak points detection: From the starting point, follow the boundary in clockwise direction and search for the first peak point encountered ($P_{Peak1}$). Again, from the starting point, follow the boundary in anticlockwise direction and search for the first peak point encountered ($P_{Peak2}$). Peak point is defined as the point in which it has the smallest Y-coordinate value in compare to all the D proceeding points. D is the number of next-of-point to be tested. Refer to Fig. 11(b) for better understanding.
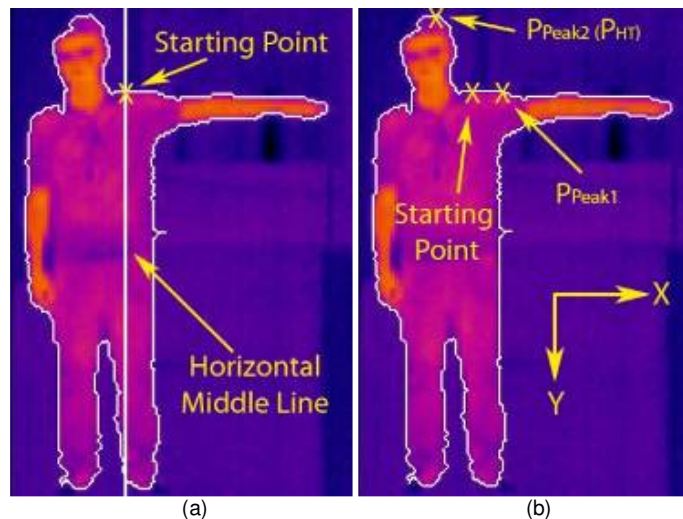
**FIGURE 11:** (a)Horizontal middle line and the starting point as in step1. (b) Detection of (c/w from Starting point) and (couter c/w from starting point)

Step 3: Head top point detection: Compare $P_{Peak1}$ and $P_{Peak2}$ obtained in step 2. Record the highest point (with smaller Y-coordinate) as the head top point, $P_{HT}$. For example, in Fig. 11(b), $P_{Peak2}$ is higher than $P_{Peak1}$ . Thus $P_{HT} = P_{Peak2}$.

Step 4: Boundary line splitting: Split the boundary into left boundary (Bl) and right boundary (Br) from the head top point towards bottom. Take only one point for each y-coordinate to filter out unwanted information such as raised hands. (Refer Fig. 12 for better understanding).
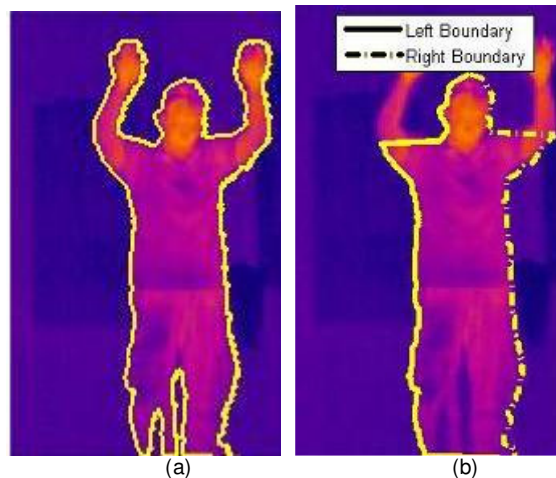


**FIGURE 12:** a) Original object boundary. (b) Left and Right object boundary after the splitting process (step 4).

$$Bl=[xl_i,yl_i] \, , \, Br=[xr_i,yr_i] \qquad (9)$$

Where $xl_i,yl_i,xr_i,yr_i$ are the pixels' y-coordinates and x-coordinates for left boundary and right boundary respectively.

I=1…N is the index number.

N=size of the boundary matrix (N is the number of pixels for left and right boundary)

Step 5: Left significant points detection: Search downwards along left boundary (Bl) from $P_{HT}$ for the first leftmost point encountered ($Pl_p$). Next, search for the rightmost point right after $Pl_p$ which is $Pl_d$. Refer Fig. 13 for better understanding.

$$Pl_p=(xl_{lp}, \, yl_{lp}), \, Pl_d=(xl_{ld}, \, yl_{ld}) \qquad (10)$$

Where subscript lp = index number of the first leftmost point

Subscript ld = index number of the rightmost point right after $Pl_p$

Step 6: Right significant points detection: Search downwards along right boundary (Br) from $P_{HT}$ for the first rightmost point encountered ($Pr_p$). Next, detect the leftmost point right after $Pr_p$ which is $Pr_d$. Refer Fig. 6 for better understanding.

$Pr_p=(xr_{rp}, yr_{rp})$, $Pr_d=(xr_{rd}, yr_{rd})$     (11)

Where subscript rp = index number of the first rightmost point

subscript rd = index number of the first leftmost point right after $Pr_p$
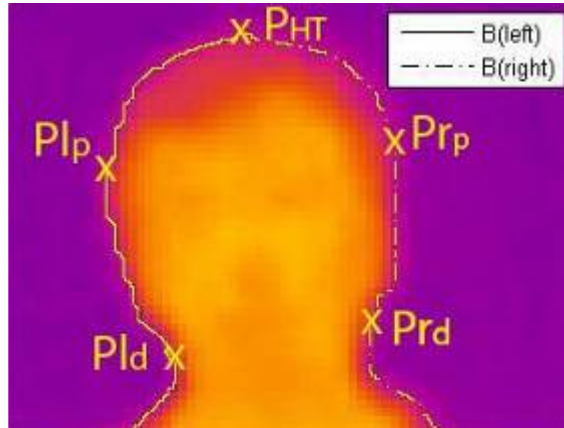


**FIGURE 13:** Example of points found in step 3, step 5 and step 6.

Step 7:  Head symmetric test:

Define $h_l$ = Vertical distance between $P_{HT}$ and $Pl_d$

$h_r$ = Vertical distance between $P_{HT}$ and $Pr_d$

Test the ratio between $h_l$ and $h_r$. If $h_l/h_r$ or $h_r/h_l > 2$, then this object is not considered as a human being and we can skip the next subsequent steps in this algorithm and proceed with the next object. Else, the object has the possibility to be considered as a human being. Continue step 8 for further detection.

Step 8: Neck-body position test: Calculate $\Delta x$, which is the distance between $x_c$ and $x_m$ where $x_c$ = horizontal center between $Pl_d$ and $Pr_d$ and $x_m$ is obtained in step1.

Define $w_n$ =horizontal distance between $Pl_d$ and $Pr_d$.

If $\Delta x \geq 2w_n$, then this object is not considered as a human being and we can skip the next subsequent steps in this algorithm and proceed with next object. Else if $\Delta x < 2w_n$ , then the object has the possibility to be considered as a human being. Continue step 9 for further detection.

Step 9: Curve tests:

I)     TOP CURVE TEST.

Define $s_t$=floor(min(lp,rp)/(F/2)) as the step size for top curve test.

Calculate:

$$C_{tl} = \begin{cases} 1, yl_{1+s_t*k} \leq yl_{1+s_t*(k+1)} \\ \quad 0, otherwise \end{cases}$$

$$C_{tr} = \begin{cases} 1, yr_{1+s_t*k} \leq yr_{1+s_t*(k+1)} \\ \quad 0, otherwise \end{cases} \quad (12)$$

$$C_t = \sum C_{tl} + \sum C_{tr}$$

where  k=0, …,F/2-1

F is the step size partition variable. F is even integer and F≥2.

For example, if F=6,$s_t$=8, then the y-coordinates tested is as shown in Fig. 14. The same concept goes for left curve test and right curve test.
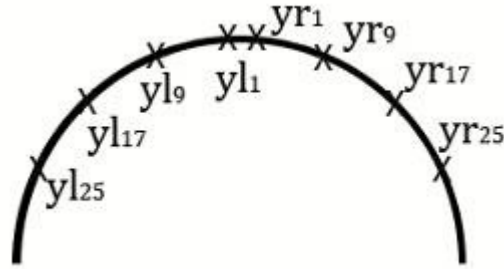
Note: the symbol '*' means multiply.

**FIGURE 14:** Example on top curve test.

II)    LEFT CURVE TEST

Define $s_l$ = floor(min(lp,ld-lp)/(F/2)) as the step size for left curve test.
Calculate:

$$C_{l1} = \begin{cases} 1, xl_{lp+s_l*k} \leq xl_{lp+s_l*(k+1)} \\ \quad\quad 0, \text{otherwise} \end{cases}$$

$$C_{l2} = \begin{cases} 1, xl_{lp-s_l*k} \leq xl_{lp-s_l*(k+1)} \\ \quad\quad 0, \text{otherwise} \end{cases} \quad (13)$$

$C_l = \sum C_{l1} + \sum C_{l2}$
where k=0, …,F/2-1

III)    RIGHT CURVE TEST

Define $s_r$ = floor(min(rp,rd-rp)/(F/2)) as the step size for right curve test.
Calculate:

$$C_{r1} = \begin{cases} 1, xr_{rp+s_r*k} \geq xr_{rp+s_r*(k+1)} \\ \quad\quad 0, \text{otherwise} \end{cases}$$

$$C_{r2} = \begin{cases} 1, xr_{rp-s_r*k} \geq xr_{rp-s_r*(k+1)} \\ \quad\quad 0, \text{otherwise} \end{cases} \quad (14)$$

$C_r = \sum C_{r1} + \sum C_{r2}$
Where k=0, …,F/2-1

Step 10: Human identification:
Define curve test condition:
$C_t \geq F-1$            - (15)
$C_l \geq F-1$            - (16)
$C_r \geq F-1$            - (17)
Check condition (15),(16) and (17). If any two or more conditions are true, the object is verified as a human being. Else, the object is not considered as a human being.

## 5. HOME ALONE FAINT DETECTION ALGORITHM

In this section, an effective faint detection algorithm for monitoring home alone personal is proposed for the omnidirectional thermal imaging surveillance system.

Step 1: Global parameters definition: Define global parameters to be used in the designed algorithm such as $Hp$ = human's height in previous image, $Hc$ = human's height in current image, $Wp$ = human's width in previous image and $Wc$ = human's width in current image, $f$ = accumulator for human lying image, $F$ = total frames (time) to decide whether a human being is fainted, $S$ = smallest possible human being's size (in terms of number of pixels in group) in an image, $Hmax$ = maximum height of human of image being capture and initialize it to 0.

Step 2: Image acquisition: Acquire image of background image from thermal camera, unwarp it and store as RGB image, $B$. Acquire image from thermal camera, unwarp it and store as RGB image, $I$. An example of $B$ and $I$ is shown in Fig 15.
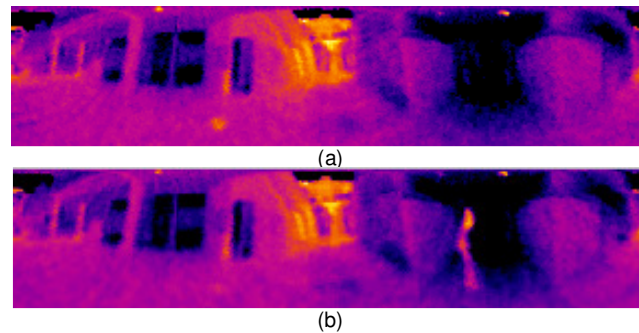
(a)



(b)

**FIGURE 15:** Thermal image capture on site corresponding (a) Example of *B* (b) Example of *I*

Step 3: Background subtraction: Subtract image *B* from image *I* and store it as image, *Im.*

Step 4: *Binary image conversion:*
    a) Convert *Im* to gray scale image, *G*. An example of G shown in Fig 16
    b) Convert *G* to binary image, $B_1$ using minimum possible human body temperature threshold, *T*. An example of $B_1$ shown in Fig 17.

Step 5: *Noise Filtering:*
    a) Removes from $B_1$ all connected components (objects) that have fewer than *S* pixels, producing another binary image, $B_2$. An example of $B_2$ is shown in Fig. 18.
    b) Creates a flat, disk-shaped structuring element, *SE* with radius, *R*. An example of structuring element is shown in Fig. 19.
    c) Performs morphological closing on the $B_2$, returning a closed image*, $B_3$*. Morphological definition for this operation is dilates an image and then erodes the dilated image using the same *SE* for both operations. An example of $B_3$ shown in Fig. 20.
    d) Perform Hole Filling in $B_3$ and returning a filled image *A*: A hole may be defined as a background region surrounded by a connected border of foreground pixels. An example of *A* shown in Fig. 21.

Step 6: Human's height statistical search: Summing each pixels contents in every single column of *A* to form a statistical model as shown in Fig 22(a). From the statistical model, search for $H_c$ (the highest value in the plot). An example of searching $H_c$ is shown in Fig 23.

Step 7: Human's width statistical search: Summing each pixels contents in every single rows of *A* to form a statistical model as shown in Fig 22(b). From the statistical model, search for $W_c$ (the highest value in the plot). An example of searching $W_c$ is shown in Fig 23.

Step 8: If $H_c > H_{max}$, set $H_c = H_{max}$.

Step 9: *Faint detection:*
    IF $H_c \geq W_c$ and $H_c \geq$ (95% of $H_{max}$)
      THEN the human is considered standing or walking. Continue on step 10.
    IF $H_c \geq W_c$ and $H_c <$ (95% of $H_{max}$)
      THEN the human is considered fall down. Continue on step 10.
    IF $H_c < W_c$ and $W_c \neq W_p$ and/or $H_c \neq H_p$ and $f < F$,
      THEN the human is fall down. Continue on step 10.
    IF $H_c < W_c$ and $W_c = W_p$ and $H_c = H_p$ and $f < F$,
      THEN the human is considered possible faint. Continue on step 11.
    IF $H_c < W_c$ and $W_c = W_p$ and $H_c = H_p$ and $f \geq F$,
      THEN the human is considered faint. Continue on step 12.

Step 10: Reset fainted frame counter and start new cycle: Set $f = 0$, update $H_p = H_c$ and $W_p = W_c$. Repeat step 2.

Step 11: Increase frame counter by 1 and start new cycle: Set $f = f + 1$, update $H_p = H_c$ and $W_p = W_c$. Repeat step 2.

Step 12: *Faint case:* Signals alarm until operator noted and performs rescue action and resets the system manually.

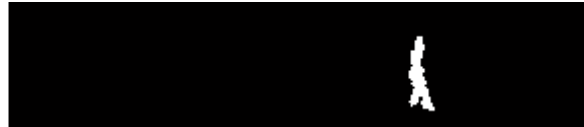**FIGURE 16:** Example of image *G*



**FIGURE 17:** Example of image *B1*
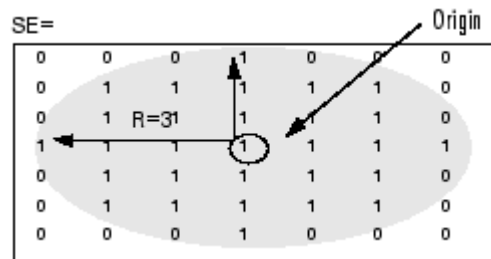


**FIGURE 18:** Example of image *B2*



**FIGURE 19:** Disk shaped structuring elements
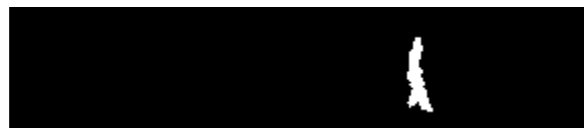


**FIGURE 20:** Example of image *B3*
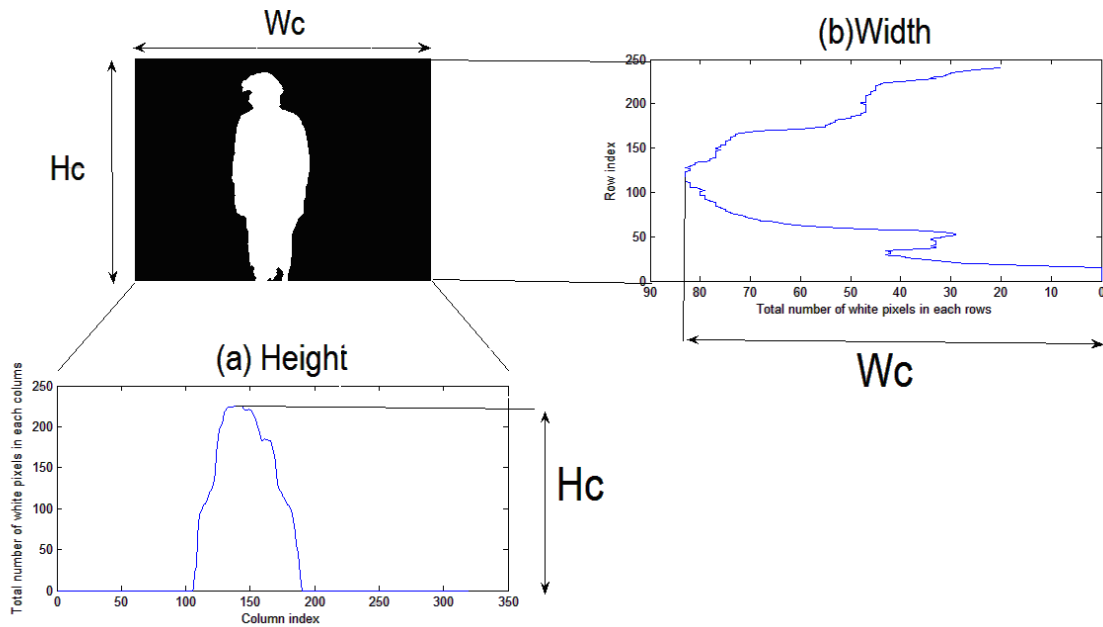


**FIGURE 21:** Example of image *A*

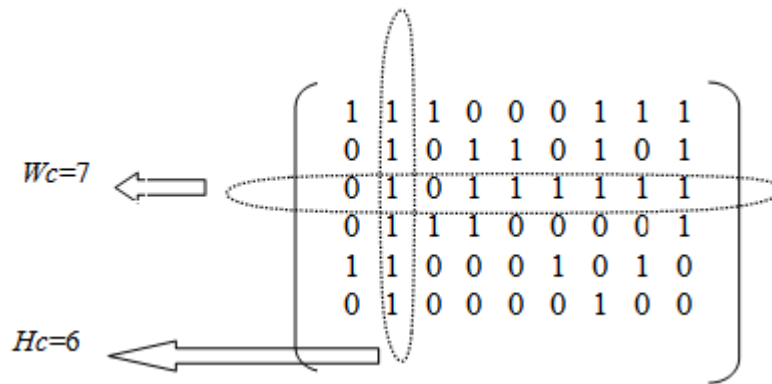**FIGURE 22:** Statistical models: (a) human height statistical search and (b) human width statistical search.



**FIGURE 23:** Examples of searching *Hc* and *Wc*

## 6. EXPERIMENTAL RESULTS

In this section, the application of the proposed omnidirectional thermal imaging system for trespasser and faint detection are briefly illustrated. The omnidirectional thermal images for a wide area test site are collected at the main office entrance in Faculty of Engineering and Technology (FET), Multimedia University. An omnidirectional image captured by using digital camera on the site is shown in Fig. 24. An omnidirectional thermal image is also captured by using thermal camera on the site is shown in Fig. 25. The unwarped form of Fig. 24 (digital color panoramic form) is shown in Fig. 26 whereas the unwarp form of Fig. 25 (thermal image panoramic form) is shown in Fig. 27 respectively. In Fig. 27, the log-polar mapping process is by 4:1 reduction mapping scale, which means that 320 X 240 omnidirectional thermal image's Cartesian pixels are mapped to one fourth of the thermal image Cartesian pixels (320 X 60) in panoramic view, with four fold data compression compare to original omnidirectional thermal image as in Fig. 25. The captured thermal images are tested for trespasser and faint detection algorithm proposed in section 4 and 5 in the subsection below.

*A.)  Experimental Test on Human Head Detection Algorithm for Trespasser Detection*

A series of experiment is done to determine the optimum parameters stated in the human head detection algorithm and to examine the performance of the algorithm in its optimum setting. The

**FIGURE 24:** Case studies of trespasser and faint detection captured at main office entrance in FET (digital color form).
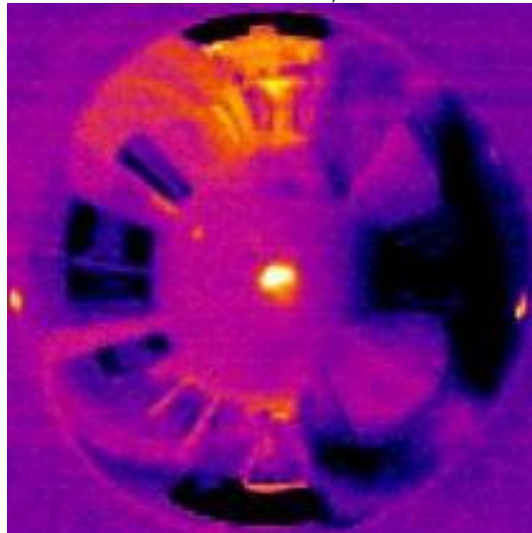


**FIGURE 25:** Case studies of trespasser and faint detection captured at main office entrance in FET (thermal image).



**FIGURE 26:** Unwarp form of Fig. 24 (digital color panoramic form)
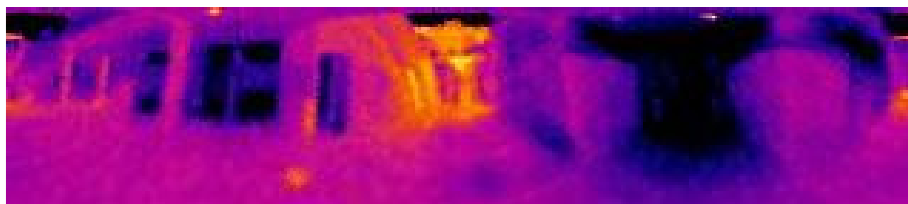


**FIGURE 27:** Unwarp form of Fig. 25 (thermal image panoramic form)

testing site is the main office entrance of Faculty of Engineering and Technology, Multimedia University, which simulates the door of a nursing home, for tracking Alzheimer patients from leaving nursing home without permission and theft during night time. The omnidirectional thermal imaging tool is setup with the height of 1.5m. This setting is chosen because it gives the best view of the testing site. A total of 10,000 thermal images with test subjects (human being or animal) roaming randomly in the area visible to the proposed system are taken.

To determine optimum value for parameter $T_l$, a random sample image is chosen and converted into B&W image using step 2 of the Algorithm for Trespasser Detection with value of $T_l$ ranging from 0 to 510 (sum of R and G component in RGB image. B component is excluded because it is not proportional to the change of temperature). Perform the binary image conversion repeatedly with increasing step size of 10 for $T_l$ and search for the optimum $T_l$ where the noise can be minimized and the human is not distorted in the resulting image. The optimum setting found for $T_l$ is 150 in this experiment. For example, if $T_l =130$ is used, excessive noise will be introduced. If $T_l =170$ is used, there will be too much distortion to human being in the resulting image. Refer Fig. 28 for better understanding.
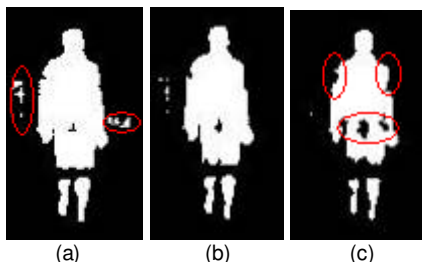


**FIGURE 28:** (a) $T_l =130$ (b) $T_l =150$ (c) $T_l =170$.

To determine the optimum value for parameter $T_h$, perform the binary image conversion repeatedly with decreasing step size of 10 for $T_h$ and search for the minimum value of $T_h$ which does not influence the appearance of the human object. The optimum value found for $T_h$ is 430 in this experiment. For example, if $T_h =400$ is used, the image of human being is distorted. If $T_h =460$ is used, there will be no improvement for the image. Lower $T_h$ value is preferred because it will filter out more high temperature noise component. Refer Fig. 29 for better understanding.



**FIGURE 29:** (a) $T_h =400$ (b) $T_h =430$ (c) $T_h =460$.

The accuracy of the proposed algorithm is then evaluated using 'operator perceived activity' (OPA) in which the proposed algorithm is evaluated with respect with the results interpreted by a human observer [7],[23]. Firstly, the thermal images are tested using the proposed algorithm. Then, the result is compared with the result of the human observer. The accuracy of the proposed algorithm is the percentage of interpretation (trespasser or not) agreed by both the human observer and the proposed algorithm.
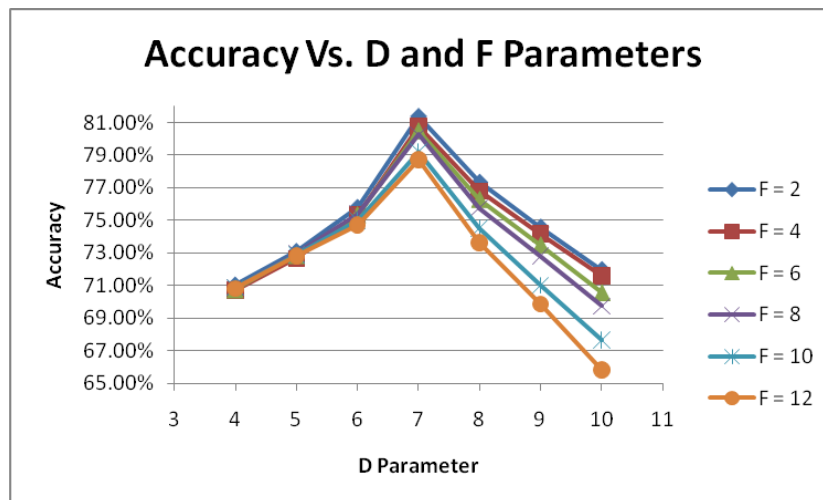
**FIGURE 30:** Accuracy of proposed algorithm for different combination of D and F.

To determine parameter D and F, all of the 10,000 images in group 1 are tested with different combinations of D and F. As shown in the graph in Fig. 30, the optimum value for parameter D and F are 7 and 2 which contribute to accuracy of 81.38%. From the observation, the smallest the step size partition variable (F), the accurate the trespasser detection is. D is optimum at 7 proceeding points, more than 7 proceeding points or lesser will degrade the overall performance of the trespasser detection accuracy. The proposed algorithm is able to operate in a very fast manner whereby the routine time required to capture a thermal image, unwarped into panoramic form, detect the existence of a trespasser and trigger the alarm is only 2.27 seconds.

*B.) Experimental Test on Home Alone Faint Detection*

In this section, the proposed algorithm for faint detection will be briefly discussed. The testing site is at the lobby around the main entrance of the Faculty of Engineering and Technology, Multimedia University, which simulates the activities area of a nursing home/hospital. For experimental purpose, 17,878 sample images include background image had been captured to test the accuracy of the proposed faint detection algorithm. At the test site, omnidirectional thermal images had been captured using the omnidirectional thermal imaging system, unwarped into panoramic form, performed image filtering, image processing for faint detection and signal alarm or not. These images included different poses of human such as standing or walking, falling, and fainting. The system routine time including the time for capture in omnidirectional thermal image, unwarping into panoramic form, image filtering, faint detection and signal alarm or not is 1 frame per second. Thus *F* as an example is set to 7 so that if a person lies on the same place with same size for 7 second, the system will classify the person is fainting.

The thermal image temperature range has been set from 25°C to 38°C. Human shape's parameters *S* and *R* are approximate from one of the testing image at a distance of 5 meters from the imaging system. From that image, the human's total pixels are only 30. Hence, *S* is set to 30 and *R* for *SE* is set to 2 respectively. Then, different *T* are tried in order to get the approximate human shape. *T* found to be falls within the range of 100 to 126. The *T* value depends on the temperature of the environment. At night time, *T* value is about 120 to 126, whereas in the afternoon, the *T* value is about 100 to 120.

Some example images of different human poses are shown in Fig. 31-33 (each for standing, falling (bending body) and fainting respectively). To differentiate between human standing motion and human bending body motion, a parameter, *p* has been set according to the factor of *Hmax*. The *p* value are found achieved highest accuracy when *p* = 95% of *Hmax* from Fig 6.14. Hence *p* value was set to 95% of *Hmax*. The proposed algorithm had been tested at night time with poor lighting condition at outdoor. The table I show the accuracies of the proposed faint detection algorithm on site.
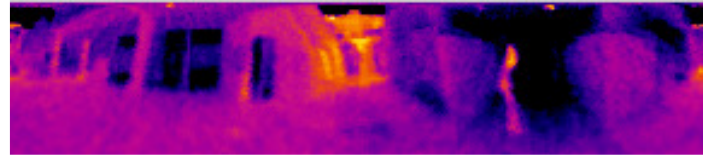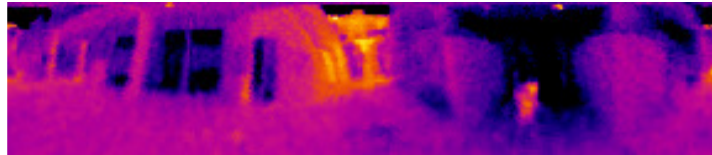
(a)



(b)

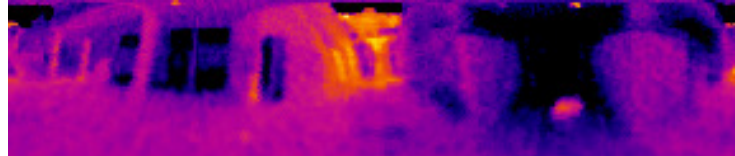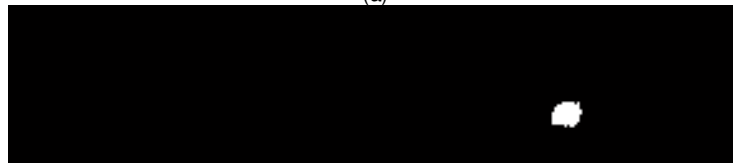**FIGURE 31:** Standing motion (a) Thermal image  (b) Black and white image



(a)



(b)

**FIGURE 32:** Falling/bending body motion (a) Thermal image  (b) Black and white image



(a)



(b)

**FIGURE 33:** Fainting motion (a) Thermal image  (b) Black and white image
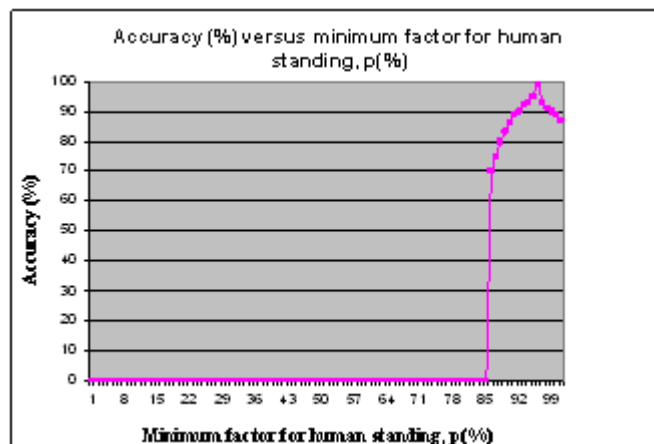
Fig. 34: Graph of accuracy versus *p*

| Motion | Test frames | Success | Fail | Accuracy (%) |
|---|---|---|---|---|
| Standing , walking | 6550 | 6498 | 52 | 99.20 |
| Falling | 4578 | 3983 | 595 | 86.78 |
| Fainting | 6750 | 6043 | 707 | 89.50 |
| **Total** | 17878 | 16524 | 1354 | 92.42 |

TABLE I. OUTDOOR MOTION DETECTION AT NIGHT WITH POOR AMBIENT LIGHT CONDITION

The results in table I show that standing or walking motion has highest accuracy compare to falling and fainting motion with 99.20%. The reason that falling motion has the lowest accuracy (with 86.78%) is because some of the falling motion is considered as standing motion in the proposed system. Besides, 89.5% of the fainting motion was detected correctly among the total tested images. Lastly, the proposed algorithm was well performed on poor lighting conditions at night with an average accuracy of 92.42%. Overall, the system can classify human behavioral best in normal standing or walking motion and good in detecting fainting motion as well no matter in good or poor lighting condition. The home alone faint detection surveillance system also functions in a fast way whereby the routine time required to capture in a thermal image, unwarp into panoramic form, detect whether there is a faint suspected case until the signal alarm or not is only 1.85 seconds. When there is a fainting motion detected, the alarm will be trigger until the operator performs the rescue action and resets the system manually.

## 7. CONCLUSION

In this paper, the usage of hyperbolic IR reflected mirror is proposed in a thermal imaging system for omnidirectional thermal imaging smart surveillance purposes In the proposed system, both human detection and faint detection algorithm has been implemented in order to facilitate smart surveillance functionality which is able to greatly increase the effectiveness of the surveillance system. The trespasser detection algorithm is used mainly to detect unauthorized movement to and fro the building while the faint detection algorithm is used to detect the event where human being faint inside the premise.

For human head detection algorithm, the thermal images are first converted into binary (Black and White) images. The presence of human being is then analyzed based on the shape of the objects (head detection) in the binary image. From the experimental results, it is shown that the proposed trespasser detection algorithm is able to achieve an accuracy of 81.38% with a routine time of 2.27 seconds. For home alone faint detection algorithm, it enables the faint event to be detected even in poor lighting condition. The experimental results show that the proposed faint detection algorithm in the omnidirectional surveillance system achieved high accuracy in monitoring the faint event in the poor lighting condition with the accuracy of 89.50% with a routine time of 1.85 seconds.

There are some distortion on the captured thermal image whereby the temperature surrounding will affect the accuracy for both the proposed trespasser and faint detection algorithm. For example, the temperature surrounding which is nearly equal to the human body will make the human body undistinguishable from the temperature surrounding. Besides, the clothes of the human with lower temperature (human sweating) will causes part of the actual human body temperature changed.

In future, a plan is proposed to combine visible/infrared image fusion model into the currently proposed model to improve the performance of the trespasser and faint detection. In additional to that, it is also planning to employ microprocessor modules such as FPGA (field programmable gate array) and ARM (Advanced RISC Machine) for the image processing and analyzing tasks instead of a computer to effectively reduce the costs and power consumption of the proposed system. These topics will be addressed in future works.

## 8. REFERENCES

[1]   A. Hampapur, L. Brown, J. Connell, S. Pankanti, A. Senior et al., "Smart Surveillance: Applications, Technologies and Implications", Information, Communications and Signal Processing, Vol. 2, p.p. 1133-1138.

[2]  A. Hampapur, L. Brown, J. Connell, A. Ekin, N. Haas, M. Lu et al., "Smart Video Surveillance", IEEE Signal Processing Mag., March 2005, p.p. 39-51.

[3]  M.W. Green, "The appropriate and effective use of security technologies in U.S. schools, A guide for schools and law enforcement agencies", Sandia National Laboratories, Albuquerque, NM, NCJ 178265, Sep 1999.

[4]  C. Shu, A. Hampapur, M. Lu, L. Brown, J. Connell et al., "IBM Smart Surveillance System (S3): A Open and Extensible Framework for Event Based Surveillance", in Advanced Video and Signal Based Surveillance (AVSS 2005), 2005, p.p. 318-323.

[5]  C. Lu, and M. S. Drew, "Automatic Compensation for Camera Settings for ImagesTaken Under Different Illuminants", Technical paper, School of Computer Science, Simon Fraser University, Vancouver, British Columbia, Canada, 2007, p.p. 1-5.

[6]  Thermographic camera. Retrieved from Wikipedia, the free encyclopedia Web Site: http://en.wikipedia.org/wiki/Thermal_camera.

[7]   W.K. Wong, P.N. Tan, C.K. Loo and W.S. Lim, "An Effective Surveillance System Using Thermal Camera", 2009 International Conference on Signal Acquisition and Processing (ICSAP2009) 3-5 Apr, 2009, Kuala Lumpur, Malaysia, p.p. 13-17.

[8]  M.R. Narayanan, S.R. Lord, M.M. Budge, B.G. Cellar and N.H. Novell, "Falls Management: Detection and Prevention, using a Waist-mounted Triaxial Accelerometer", 29 th Annual International Conference of the IEEE Engineering in Medicine and Biology Society, 2007, p.p.4037-4040.

[9]  J. Han and B. Bhanu, "Fusion of color and infrared video for moving human detection", ACM Portal, Pattern Recognition, p.p. 1771-1784.

[10] J. Chahl and M. Srinivasan, "Reflective surfaces for panoramic imaging", *Applied Optics*, 36(31), Nov 1997, p.p.8275-85.

[11] S. Gachter, "Mirror Design for an Omnidirectional Camera with a Uniform Cylindrical Projection when Using the SVAVISCA Sensor", Research Reports of CMP, OMNIVIEWS Project, Czech Technical University in Prague, No. 3, 2001. Redirected from: http://cmp.felk.cvut.cz/projects/omniviews/

[12] T. Svoboda, *Central Panoramic Cameras Design, Geometry, Egomotion.* PhD Theses, Center of Machine Perception, Czech Technical University in Prague, 1999.

[13] http://www.flirthemography.com

[14] J.W. Davis and V. Sharma, "Background-Subtraction in Thermal Imagery Using Contour Saliency", International Journal of Computer Vision 71(2), 2007, p.p. 161-181.

[15] H. Araujo, J. M. Dias, "An Introduction To The Log-polar Mapping", *Proceedings of 2nd Workshop on Cybernetic Vision*, 1996, p.p. 139-144.

[16] C. F. R. Weiman and G. Chaikin, "Logarithmic Spiral Grids For Image Processing And Display", *Computer Graphics and Image Processing*, Vol. 11, 1979, p.p. 197-226.

[17] LIRA Lab, Document on specification, *Tech. report*, Espirit Project n. 31951 – SVAVISCA-available at http://www.lira.dist.unige.it.

[18] R. Wodnicki, G. W. Roberts, and M. D. Levine, "A foveated image sensor in standard CMOS technology", *Custom Integrated Circuits Conf*. Santa Clara, May 1995, p.p. 357-360.

[19] F. Jurie, "A new log-polar mapping for space variant imaging: Application to face detection and tracking", *Pattern Recognition,Elsevier Science*, 32:55, 1999, p.p. 865-875.

[20] V. J. Traver, "Motion estimation algorithms in log-polar images and application to monocular active tracking", PhD thesis, Dep. Llenguatges.

[21] R. Wodnicki, G. W. Roberts, and M. D. Levine, "A foveated image sensor in standard CMOS technology", *Custom Integrated Circuits Conf*. Santa Clara, May 1995, p.p. 357-360.

[22] Ling Hooi Lee, "Smart Surveillance Using Image Processing and Computer Vision Techniques.", Bachelor Degree thesis, Multimedia University, Melaka, Malaysia.

[23] J. Owens, A. Hunter and E. Fletcher, "A Fast Model–Free Morphology–Based Object Tracking Algorithm", British Machine Vision Conference, 2002,p.p. 767-776 .